diagnostics

MDPI

Article

Diagnostic Performance of Selected MRI-Derived Radiomics Able to Discriminate Progression-Free and Overall Survival in Patients with Midline Glioma and the H3F3AK27M Mutation

Maria-Fatima Chilaca-Rosas [1], Melissa Garcia-Lezama [2], Sergio Moreno-Jimenez [3] and Ernesto Roldan-Valadez [2,4,*,†]

[1] Radiotherapy Department, Hospital de Oncología, Centro Medico Nacional Siglo XXI, Instituto Mexicano del Seguro Social, Mexico City 06720, Mexico
[2] Directorate of Research, Hospital General de Mexico "Dr Eduardo Liceaga", Mexico City 06720, Mexico
[3] Directorate of Surgery, Instituto Nacional de Neurología y Neurocirugia, "Manuel Velasco Suarez", Mexico City 14269, Mexico
[4] Department of Radiology, I.M. Sechenov First Moscow State Medical University (Sechenov University), Moscow 119992, Russia
* Correspondence: ernest.roldan@usa.net; Tel.: +5255-2789-2000 (ext. 1149)
† Current address: Dr. Balmis 148, Colonia Doctores, Delegacion Cuauhtemoc, Ciudad de México 06720, Mexico.

Abstract: Background: Radiomics refers to a recent area of knowledge that studies features extracted from different imaging techniques and subsequently transformed into high-dimensional data that can be associated with biological events. Diffuse midline gliomas (DMG) are one of the most devastating types of cancer, with a median survival of approximately 11 months after diagnosis and 4–5 months after radiological and clinical progression. Methods: A retrospective study. From a database of 91 patients with DMG, only 12 had the H3.3K27M mutation and brain MRI DICOM files available. Radiomic features were extracted from MRI T1 and T2 sequences using LIFEx software. Statistical analysis included normal distribution tests and the Mann–Whitney U test, ROC analysis, and calculation of cut-off values. Results: A total of 5760 radiomic values were included in the analyses. AUROC demonstrated 13 radiomics with statistical significance for progression-free survival (PFS) and overall survival (OS). Diagnostic performance tests showed nine radiomics with specificity for PFS above 90% and one with a sensitivity of 97.2%. For OS, 3 out of 4 radiomics demonstrated between 80 and 90% sensitivity. Conclusions: Several radiomic features demonstrated statistical significance and have the potential to further aid DMG diagnostic assessment non-invasively. The most significant radiomics were first- and second-order features with GLCM texture profile, GLZLM_GLNU, and NGLDM_Contrast.

Keywords: midline glioma; paediatric; brain tumour; radiomic; MRI; prognosis

check for updates

Citation: Chilaca-Rosas, M.-F.; Garcia-Lezama, M.; Moreno-Jimenez, S.; Roldan-Valadez, E. Diagnostic Performance of Selected MRI-Derived Radiomics Able to Discriminate Progression-Free and Overall Survival in Patients with Midline Glioma and the H3F3AK27M Mutation. *Diagnostics* **2023**, *13*, 849. https://doi.org/10.3390/diagnostics13050849

Academic Editor: Daniel Thomas Ginat

Received: 29 January 2023
Revised: 13 February 2023
Accepted: 20 February 2023
Published: 23 February 2023

Copyright: © 2023 by the authors. Licensee MDPI, Basel, Switzerland. This article is an open access article distributed under the terms and conditions of the Creative Commons Attribution (CC BY) license (https://creativecommons.org/licenses/by/4.0/).

1. Introduction

Diffuse midline gliomas (DMG) are aggressive astrocytic tumours that occur in the paediatric population, adolescents, and young adults (AYA) affected in the brainstem or midline structures [1,2]. It has a poor median survival of approximately 11 months from histopathological diagnosis and only 4–5 months after radiological and clinical progression [3,4].

Advances in molecular diagnosis have had an essential impact in refining the discrimination of tumours according to genetic characteristics. We can particularly distinguish those DMG with the H3.K27M mutation since it is associated with a worse outcome, showing a survival rate after two years lower than 10% [5].

"Radiomics" refers to the acquisition of traces of quantitative features that are usually non-perceptible to human vision and are obtained from different imaging techniques

that are subsequently transformed into high dimensional data that can be associated with biological events such as the progression of tumours in oncology [6]. Radiomics encompasses novel methods for high-throughput quantitative feature extraction from a pixel value, distribution, spatial relation, or specified region of interest (ROI) and volume of interest (VOI) from conventional and advanced imaging modalities [5], and in recent years it has been of interest in brain tumours such as gliomas.

The past decades have had a considerable impact in the medical imaging field; previously perceived qualitative-only images can now be minable quantitative data rather than pictures [7]. Furthermore, recently they have been found to predict histology, response to treatment, genetic signature, recurrence, and survival, among other features, in several pathologies, especially cancer [8,9]. In a recent meta-analysis, radiomics depicted a high level of predictive value for pre-operative lymph node metastasis in patients with biliary tract cancers; this study also showed that MRI-derived radiomics had a higher pooled sensitivity than CT [10].

Radiomics can also potentially be used for personalised therapy and the prediction of individual treatment outcomes [7,11]. Moreover, with the increasing implementation of artificial intelligence (AI) in medical imaging, this could go even further; however, this will not be further discussed as it is out of the scope of our research and implicates psychological, ethical, and medico-legal issues that need to be addressed for AI to be applicable in patient management [12].

Although radiomics demonstrated potential in survival prediction for DMG from presurgical neuroimaging using a connectome model in 2022 [13], this study did not show which specific radiomic could support the predictive ability. Overall, there is still scarce research on the subject. Until February 2023, there were only nine publications on PubMed, including "Radiomics" and "Midline gliomas or midline glioma" in their title; none of them presented a diagnostic performance test with cut-off values for specific radiomics [5,14–21].

A study published by Wagner et al. in 2023 evaluated MRI-derived radiomic features able to predict PFS and OS. It included a cohort of 89 patients; however, in their study not all patients had the histopathological and molecular diagnosis (29.2%), which, as mentioned by themselves, is inherent to most DMGs. They identified radiomics of T2-FLAIR and nonenhanced T1-weighted sequences that were predictive of PFS and GLSZ as the predominant predictive radiomic feature matrix. It was also mentioned that incorporating H3 K27M molecular markers could further increase model performance [22].

Our goal with this study was to perform a comprehensive diagnostic assessment of MRI-derived radiomics in patients diagnosed with DMG using conventional MRI sequences (T1 post gadolinium and T2) to calculate the basic diagnostic performance parameters from the set of radiomics of one of the leading oncology semi-automatised software programs [23]. Select parameters might support the assembling of specific predictive modelling using radiomic-specific cut-off values.

2. Materials and Methods

This observational retrospective HIPAA-compliant study was approved by the National Committee of Scientific Research of Oncology and paediatrics hospital of National Medical Centre S.XXI IMSS, Mexico City with No. F-CNIC-2020-321; it included patients' records with midline gliomas identified in paediatrics and AYA in the database of Research of Oncology and paediatrics hospital of National Medical Centre S.XXI IMSS, Mexico City. All the information reported followed the national and international standards for the management of clinical files (the official Mexican norm NOM-012-SSA3-201218, which establishes the criteria for the execution of scientific projects for the health of human beings) and with the Helsinki Declaration of 1975, as revised in 2013.

Inclusion criteria included a histopathological diagnosis of midline glioma with the determination of the H3.3K27M mutation according to WHO 2007 and 2016 and the tumour's location in the midline region based on magnetic resonance imaging (MRI) [12]. The exclusion criteria were concurrence with other neoplasms from 5 years ago or another

lethal comorbidity. Elimination criteria were applied to MRI studies whose DICOM files could not be downloaded for assessment. Of the initial 91 patients identified, 46 underwent a biopsy procedure but 26 presented undetermined results due to insufficient tissue samples. Two tissue samples were negative from the remaining 20 patients, and 18 were positive for the HF3K27M mutation, fulfilling the 2007 and 2016 WHO criteria for the histopathological diagnosis. Of the 18 positive patients, only 12 had available DICOM MRI files included in the analysis. The other six patients with positive HF3K27M mutation had only DICOM files of computed tomography and, therefore, were eliminated from the study. A flow diagram of the patient selection is shown in Figure 1.

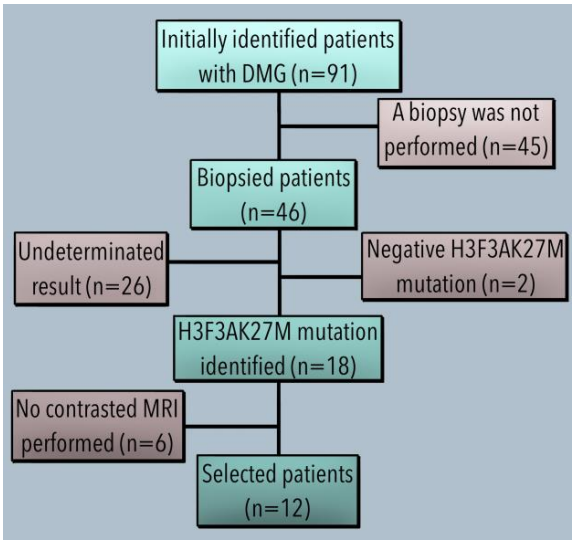


Figure 1. Patient selection process.

2.1. Imaging Evaluation of Midline Gliomas

MRI evaluations were conducted on a 1.5T Magnetom (Siemens Healthcare, Erlangen, Germany) and a 3T Magnetom (Philips Health, Hong Kong, China). Gadolinium-enhanced T1-weighted images (T1WI) covering the entire midline and T2-weighted images were acquired with 60–80-slice processing. The MRI evaluation was performed by two neuroradiologists and a radio-oncologist with over ten years of experience. The radiological features involved tumour location, peritumoral oedema and necrosis, tumour volume, and cystic changes. The T1 pre- and post-gadolinium and T2 sequences allowed the identification of morphological features (see Figure 2). The images were processed for analysis in the semiautomatic platform, and the radiomic characteristics were obtained, which were later analysed with the oncological results (see Figure 3).

2.2. Radiomics Extraction

We used the software LIFEx v7.1.0 (French Alternative Energies and Atomic Energy Commission, Orsay, France) to extract radiomic features from the brain MRI images of patients with DMG. It is a software for radiomics feature extraction in multimodality imaging. Until the writing of this article (27 January 2023), the official website for the software reported its use in 497 publications in PubMed; it also received 633 citations with special recognition in oncology [24]. The methods for using the LIFEx v7.1.0 have been previously reported and contemplate the IBSI criteria [23]. MRI images of the T1 pre- and post-gadolinium and T2 sequences were uploaded into the LIFEx to extract the radiomic characteristics; it extracted 94 different radiomics, which were grouped into three categories: shape and volume features, intensity features, and texture features. From the total of 94 radiomics extracted, 14 were eliminated from our analyses since they apply to other imaging techniques (CT, NM, and PET), leaving a total of only 80 radiomics that were included in our calculations. In each of the selected brain MRIs, three regions were

selected for extracting the radiomics: viable tumour (represented for the enhancing tumour regions in T1 post-gadolinium sequence), peritumoral oedema (visualised on T2), and equivalent midline normal tissue (EMNT) observed in both sequences. The ROI and VOI were manually drawn across all slices of the selected sequences and validated by the imaging experts.

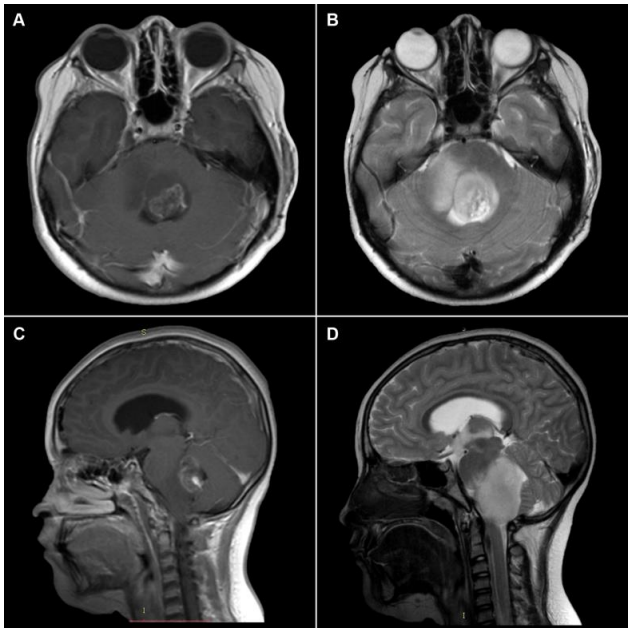


Figure 2. The axial and sagittal planes show the MRI appearance of DMG on T1- and T2-weighted images. (**A**,**C**) Images show contrast-enhanced tumoural lesions, but (**B**,**D**) images showed extensive oedema tumoural and diffuse/infiltrative patterns.

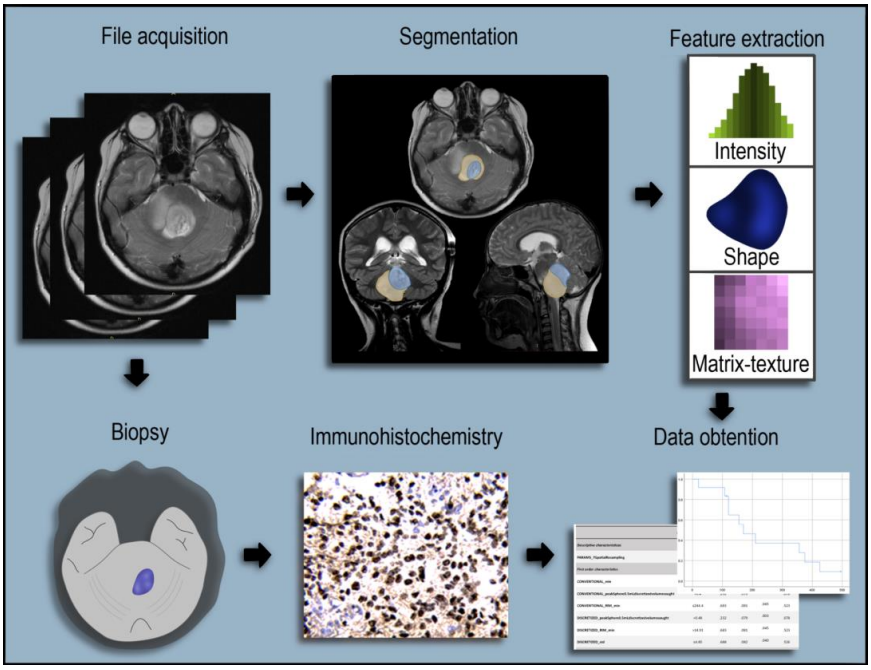


Figure 3. Description of steps followed for the data acquisition of patients. In the initial stage, patients underwent MRI imaging studies that showed pathological lesions compatible with DMG. This assessment was followed by histopathological diagnostic and nuclear immunostaining with recognition of the mutated H3F3A K27M protein. Segmentation of the tumour regions was performed. Images were uploaded into the software LIFEx for postprocessing and extraction of radiomic features.

2.3. Definitions of Progression-Free Survival and Overall Survival

PFS definition was established as the time elapsed from completing radiotherapy until tumour progression or death. The pre-operative MRI was the base for radiologists and radio-oncologists, which aided in monitoring disease evolution. The tumour recurrence report was based on the assessment of T1 post-gadolinium MRI, describing new or increased enhancing tumours within the site of initial surgical resection. RANO criteria were also considered to discriminate actual progression or recurrence against pseudoprogression when repeat pathology was unavailable. Progressive disease was defined as a $\geq$25% augmentation in enhancing tumour along with clinical deterioration requiring treatment change within six months post-RT [25]. Overall survival was defined as the time elapsed from the MRI diagnostic to the time of death from any cause [26].

2.4. Statistical Analyses

2.4.1. Descriptive Statistics and Differences between Tumour Regions

The value distribution of each radiomic was analysed using the Kolmogorov–Smirnov and Shapiro–Wilk tests. Because most of the values depicted a non-normal distribution, we used quartiles and the interquartile range (IQR) to represent the central tendency and dispersion of data. To explore simultaneous differences among regions (tumour, peritumoral oedema, and EMNT), we used the Kruskal–Wallis test followed by the Mann–Whitney U test. Significant statistical differences for ROC curve analyses were demonstrated by a p-value < 0.05.

2.4.2. Evaluation of Diagnostic Performance

Following previous publications about the diagnostic performance of quantitative brain biomarkers [27,28], the area under the ROC curve (AUROC) was considered the measurement for the overall performance for each selected GM or WM region, or GM/WM ratios [29]. Additionally, the standard error (SE), p-value, and 95% confidence interval (CI) were described. For the calculation of SE, the method of Delong [30] was applied. Other important values displayed are the sensitivity, specificity, positive and negative predictive values, and positive and negative likelihoods. Cut-off ranges served as the ideal cut-off to assess the presence of a clinical diagnosis by maximising sensitivity and specificity. To determine the accuracy, a traditionally established academic points system classification was applied as follows: 90–100% = excellent, 80–90% = good, 70–80% = fair, 60–70% = poor, and 50–60% = fail [31]. Data was presented following the Standards for Reporting of Diagnostic Accuracy (STARD) initiative [16].

2.4.3. Software

The analyses in this study were performed using IBM SPSS® (Version 27.0.0.1, International Business Machines Corp., Armonk, NY, USA) and MedCalc® (Version 20.0.15 MedCalc Software bvba, Mariakerke, Belgium).

3. Results

3.1. Demographics and Clinical Features

Of the 12 patients included, 9 were paediatric (75%) and 3 were AYAs (25%). The relation between male and female patients (M: F) was 2:1. Tumours were more frequently located in the pons (50%). The rest of the tumours were equally found in the thalamus (25%) and midbrain (25%). Patients underwent radiotherapy with a median dose of 55 Gy (ranging from 54 to 55 Gy). The radiotherapy schemes were conventional in 83.3% of patients and hypofractionated in the remaining 16.7%.

3.2. Survival Analysis

Kaplan–Meier curves showed that the median PFS was 210 days (7 months). They also depicted that the median OS was 455 days (15.2 months) in the group of patients in this study (see Figure 4).

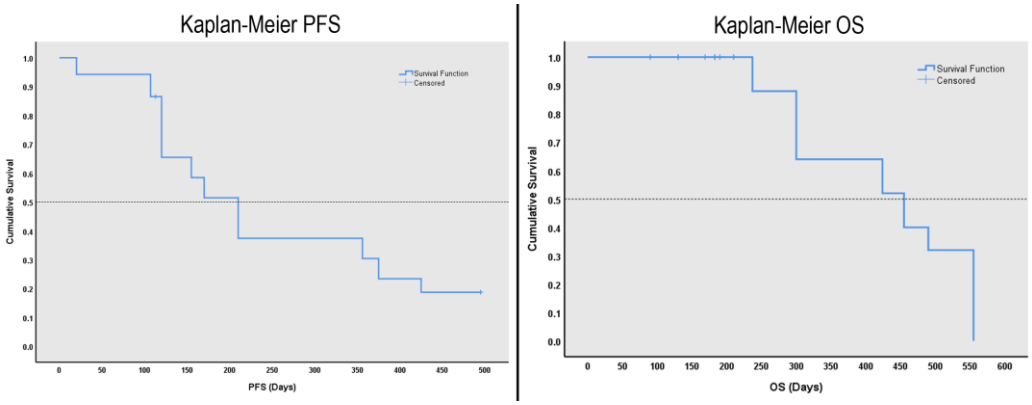


Figure 4. Survival analyses "Kaplan Meier" curves. Part (**left**) represents the curve for PFS. Part (**right**) represents the curve for OS.

3.3. Radiomic Values Differences between Tumour Regions

The Kruskal–Wallis H test was performed but did not depict any statistically significant differences between the tumour regions of each radiomic variable ($p > 0.05$).

3.4. Radiomic Values Extraction

From the three tumour regions of DMG (viable tumour, peritumoral oedema, and EMNT), 80 radiomics were obtained from each region. These measurements represented 240 radiomic features for the T1 post-gadolinium and 240 radiomics for the T2 sequence per patient. A total of 5760 radiomic values were included in the analyses. Table 1 shows the quartiles and IQR for the selected radiomics.

Table 1. Quartiles and IQR for the selected radiomics.

Radiomic Features	Percentile			IQR
	Median	75	25	
CONVENTIONAL_min	128.294	189.296	4.032	185.264
CONVENTIONAL_peakSphere0.5mL: discretised volume sought	0.506	0.522	0.472	0.05
CONVENTIONAL_RIM_min	257.726	337.008	160.108	176.972
CONVENTIONAL_RIM_stdev	70.049	106.502	32.110	74.392
CONVENTIONAL_RIM_Volume(vx)	1528.486	2413.208	783.969	1629.293
DISCRETIZED_std	4.516	5.733	2.995	2.738
DISCRETIZED_Q1	15.500	19.75	10	9.75
DISCRETIZED_peakSphere0.5mL: discretised volume sought	0.506	0.522	0.472	0.05
DISCRETIZED_peakSphere1mL: discretised volume sought	1.041	1.045	1.014	0.031
DISCRETIZED_RIM_min	13.551	250.895	7.077	243.818
PARAMS_YSpatialResampling	0.654	4.864	0.5	4.364
GLCM_Contrast[=Variance]	10.566	22.434	0.046	22.388
GLCM_Correlation	0.606	5.745	0.484	5.261
GLCM_Entropy_log10	2.071	2.368	0.567	1.801
GLCM_Entropy_log2[=JointEntropy]	6.878	7.868	2.230	5.638
NGLDM_Contrast	0.027	0.084	0.001	0.083
GLZLM_GLNU	169.238	68,327.15	65.305	68,261.845

3.5. Radiomics with Significant AUROCs to Identify PFS and OS above the Median

Our analysis showed 13 radiomics with a statistically significant difference in AUROC (p-value < 0.05). See Table 2 part A for the list of significant radiomics discriminating PFS. We found ROC curves for four radiomics with a statistically significant difference in AU-

ROC (p-value < 0.05). See Table 2 part B for the list of significant radiomics discriminating OS. Figure 5 shows the performed ROC curves.

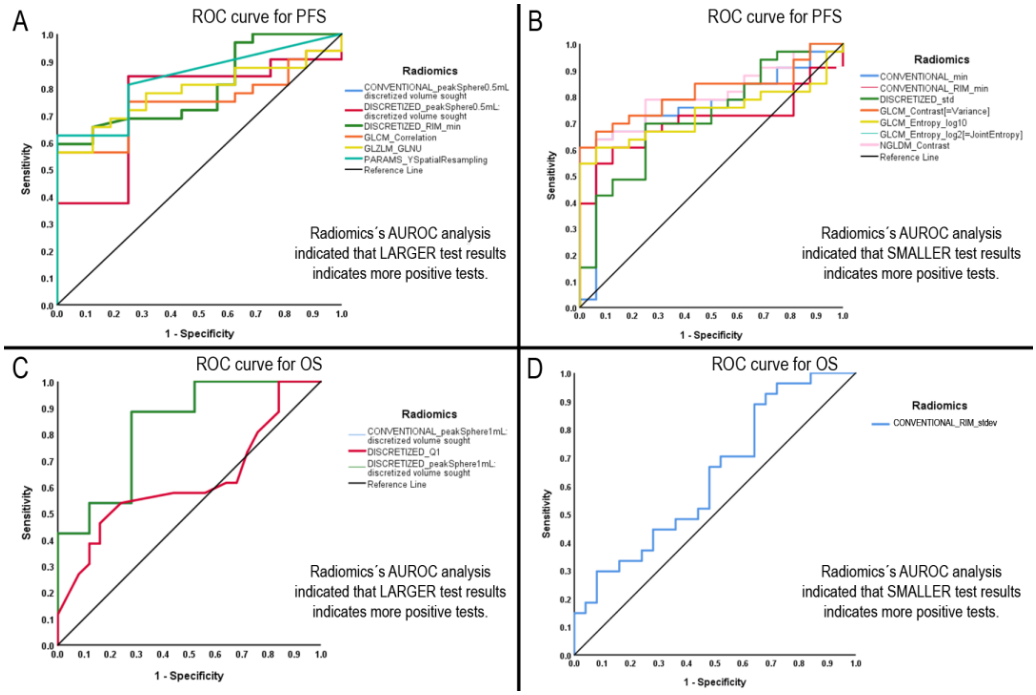


Figure 5. ROC curves of the significant radiomics. Sections (**A**,**B**) show the radiomics with significance for progression-free survival; (**C**,**D**) show the radiomics with significance for overall survival above the median.

Table 2. The cut-off value for the significant radiomic features.

Radiomic Feature	Cut-Off Value	AUROC	SE	p-Value	95% CI	
					Lower	Upper
Progression-free survival						
Descriptive characteristics						
PARAMS_YSpatialResampling	>0.65	0.188	0.064	0.001	0.062	0.313
First-order characteristics						
CONVENTIONAL_min	≤100.8	0.763	0.078	0.004	0.611	0.916
CONVENTIONAL_peakSphere0.5mLdiscretizedvolumesought	>0.4	0.232	0.079	0.003	0.078	0.386
CONVENTIONAL_RIM_min	≤244.4	0.683	0.081	0.045	0.523	0.843
DISCRETIZED_peakSphere0.5mLdiscretizedvolumesought	>0.48	0.232	0.079	0.003	0.078	0.386
DISCRETIZED_RIM_min	>14.91	0.683	0.081	0.045	0.523	0.843
DISCRETIZED_std	≤4.85	0.688	0.082	0.040	0.526	0.849
Second-order characteristics						
GLCM_ContrastVariance	≤6.12	0.781	0.069	0.002	0.647	0.916
GLCM_Correlation	>0.69	0.290	0.077	0.022	0.138	0.442
GLCM_Entropy_log10	≤1.57	0.685	0.079	0.043	0.530	0.841
GLCM_Entropy_log2JointEntropy	≤5.23	0.685	0.079	0.043	0.530	0.841
GLZLM_GLNU	>232.13	0.246	0.072	0.005	0.104	0.387
NGLDM_Contrast	≤0.02	0.775	0.069	0.003	0.639	0.910
Overall survival						
First-order characteristics						
CONVENTIONAL_peakSphere1mLdiscretizedvolumesought	>1.02	0.134	0.054	<0.001	0.029	0.240
CONVENTIONAL_RIM_stdev	≤106.56	0.686	0.080	0.035	0.529	0.843
DISCRETIZED_Q1	>17	0.321	0.083	0.042	0.160	0.483
DISCRETIZED_peakSphere1mLdiscretizedvolumesought	>1.02	0.134	0.054	<0.001	0.029	0.240

3.6. Diagnostic Performance Test

According to the mentioned traditional academic points system, our assessment found that 9 out of the 13 significant radiomics showed excellent specificity for PFS. For sensitivity, one radiomic fell under the excellent (above 90%) category (CONVENTIONAL_peakSphere0.5mLdiscretizedvolumesought), and there was one in the good (80–90%) category (DISCRETIZED_peakSphere0.5mLdiscretizedvolumesought).

For OS, three out of four significant radiomics demonstrated good (80–90%) sensitivity (CONVENTIONAL_peakSphere 1mLdiscretizedvolumesought, CONVENTIONAL_RIM_stdev and DISCRETIZED_peakSphere 1mLdiscretizedvolumesought); only the radiomic DISCRETIZED_Q1 showed fair (70–80%) specificity on the performance test. A complete description of the diagnostic performance tests is presented in Table 3.

Table 3. Diagnostic performance test evaluation for the selected radiomics.

	Radiomic (Significant AUROC)	Sensitivity		Specificity		+LR		−LR		+PV		−PV	
		Value	95% CI	Value	95% CI	Value	95% CI	Value	95% CI	Value	95% CI	Value	95% CI
PFS	CONVENTIONAL_min	63.8%	46.2–79.1%	93.7%	69.7–99.8%	10.2%	1.5–69.2%	0.3%	0.2–0.6%	95.8%	77.2–99.3%	53.7%	42.3–64.4%
	CONVENTIONAL_peakSphere 0.5mLdiscretizedvolumesought	97.2%	85.4–99.9%	0%	0–20.5%	0.9%	0.9–1%	-	-	68.6%	67.4–69.8%	0%	-
	CONVENTIONAL_RIM_min	58.3%	40.7–74.4%	93.7%	69.7–99.8%	9.3%	1.3–63.5%	0.4%	0.2–0.6%	95.4%	75.5–99.3%	50%	39.9–60%
	DISCRETIZED_peakSphere0.5mL discretizedvolumesought	83.3%	67.1–93.6%	50%	24.6–75.3%	1.6%	1–2.7%	0.3%	0.1–0.8%	78.9%	69.2–86.2%	57.1%	35.6–76.2%
	DISCRETIZED_ RIM_min	63.8%	46.2–79.1%	93.7%	69.7–99.8%	10.2%	1.5–69.2%	0.3%	0.2–0.6%	95.8%	77.2–99.3%	53.5%	42.3–64.4%
	DISCRETIZED_std	63.8%	46.2–79.1%	75%	47.6–92.7%	2.5%	1–6.1%	0.4%	0.2–0.8%	85.1%	70.3–93.2%	48%	35.4–60.7%
	GLCM_ ContrastVariance	52.7%	35.4–69.5%	100%	79.4–100%	-	-	0.4%	0.3–0.6%	100%	-	48.4%	39.9–57.0%
	GLCM_Correlation	52.7%	35.4–69.5%	93.7%	69.7–99.8%	8.4%	1.2–57.7%	0.5%	0.3–0.7%	95%	73.5–99.2%	46.8%	37.9–56%
	GLCM_Entropy_log10	47.2%	30.4–64.5%	100%	79.4–100%	-	-	0.5%	0.3–0.7%	100%	-	45.7%	38.2–53.4%
	GLCM_Entropy_ log2JointEntropy	47.2%	30.4–64.5%	100%	79.4–100%	-	-	0.5%	0.3–0.7%	100%	-	45.7%	38.2–53.4%
	GLZLM_GLNU	52.7%	35.4–69.5%	93.7%	69.7–99.8%	8.4%	1.2–57.7%	0.5%	0.3–0.7%	95%	73.5–99.2%	46.8%	37.9–56%
	NGLDM_Contrast	55.5%	38–72%	93.7%	69.7–99.8%	8.8%	1.3–60.6%	0.4%	0.3–0.6%	95.2%	74.5–99.2%	48.3%	38.9–57.9%
	PARAMS_ YSpatialResampling	58.3%	40.7–74.4%	75%	47.6–92.7%	2.3%	0.9–5.6%	0.5%	0.3–0.8%	84%	68.2–92.7%	44%	33.1–56.3%
OS	CONVENTIONAL_ peakSphere1mLdiscretized volumesought	85.1%	66.6–95.8%	60%	38.6–78.8%	2.1%	1.2–3.5%	0.2%	0.09–0.6%	69.6%	58.1–79.2%	78.9%	58.9–90.7%
	CONVENTIONAL_RIM_stdev	85.1%	66.2–95.8%	36%	17.9–57.4%	1.3%	0.9–1.8%	0.4%	0.1–1.1%	58.9%	50.7–66.7%	69.2%	44.1–86.4%
	DISCRETIZED_Q1	51.8%	31.9–71.3%	76%	54.8–90.6%	2.1%	0.9–4.7%	0.6%	0.4–0.9%	70%	51.5–83.6%	59.3%	48.2–69.6%
	DISCRETIZED_ peakSphere1mLdiscretized volumesought	85.1%	66.2–95.8%	60%	38.6–78.8%	2.1%	1.2–3.5%	0.2%	0.09–0.6%	69.6%	58.1–79.2%	78.9%	58.9–84.4%

4. Discussion

DMG is one of the most devastating types of cancer, in which its intrinsic location contributes to a poor prognosis. Recent findings have entirely revolutionised the knowledge of this disease, such as the H3.K27M mutation in up to 70% of DMG samples. However, despite the new findings, clinical trials of promising therapies, and current management involving radiotherapy and chemotherapy, the overall oncological results are still limited as the 2-year survival rate remains <10% [1,3]. In the last decade, quantifications of multiple biological events have been sought in this new area of knowledge and, in the case of neuro-oncology, with a more significant challenge of establishing objectives such as: (A) differential diagnosis, as published by Suh H. et al. 2018, between tumours glial and central nervous system lymphomas; (B) types of grade focusing on glial astrocytic tumours, the differentiation of low-grade vs. high-grade tumours; (C) vascularity mapping; and (D) responses to treatments (progression vs. pseudo-progression) [32–35].

Although preliminary radiomics studies have shown promising results related to oncology results, such as survival [36], there is no consensus for its semi-automated or complete automated application. Most published radiomics studies present signatures (clinical results with radiomic models) in addition to using an independent test set. It is a

semi-automated system with segmentation by neuroimaging, and neuro-oncology experts have proposed a tendency toward acceptance [37].

Wagner et al. presented a study of a conditional survival forest model applied to predict progression-free survival (PFS) using training data. Among their findings for PFS, the best FLAIR radiomics model yielded a concordance of 0.87 at four months, the best T1-weighted radiomics model yielded a concordance of 0.82 at four months, and the best combined FLAIR + T1-weighted radiomics model yielded a concordance of 0.74 at three months PFS [22]. However, molecular markers such as the H3K27M mutation were not incorporated due to the partial lack of biopsies in their cohort. This emphasises the importance of continuing this research line and further establishing non-invasive diagnostic/prognostic parameters that may aid clinicians.

In this study, we were able to complete the aims proposed at the beginning of this manuscript: to identify which radiomics extracted with the software LIFEx were able to discriminate PFS and OS in patients with DMG and the H3F3AK27M mutation and to obtain a comprehensive diagnostic performance assessment of those selected radiomics. The clinical relevance of this study consists of identifying cut-off values for 17 radiomics with statistical significance. From 70 radiomics initially evaluated, 13 radiomics were significant in determining patients with PFS, whereas four radiomics were significant in discriminating patients above the median of OS.

The radiomic characteristics were obtained in sequence: description characteristics, first-order statistics (histogram representation of ROI and VOI and calculation of mean, percentile, skewness entropy, and kurtosis), as well as second-order statistics (mainly assess patterns related to spatial distribution and co-occurrence of pixels and voxels) and later deriving to the radiomic characteristics of standard textures: grey-level co-occurrence matrix (GLCM) and grey-level run-length matrix (GLRM) [38]. With the analyses mentioned above, we can generate valuable information that is not perceived by human perception and that translates data from the tumour microenvironment to us [39,40], providing information that would have great predictive potential, such as the results and trends that we present in this paper [41].

In our research, the description characteristic related to the progression of cases such as PARAMS YSpatialResampling is associated with the voxel dimension in the images, for which it would be essential to resume the use of digital imaging terms in daily clinical practice with the medical images of the patients and the relevance of voxel. Further, four radiomics derived from GLCM were significant; contrast variance (of heterogeneity that gives more weight to pairs of different intensity levels that depart from the mean), correlation (shows the linear dependency of grey-level values to their corresponding voxels in the GLCM), entropy (a statistical measure of randomness), and joint entropy (a measure of the randomness/variability in neighbourhood intensity values) [42]. Regarding the second-order radiomic characteristics that have been evaluated with greater solidity in survival prognosis since the work of Molina et al. 2016, it has been with low levels of GLCM_ entropy and GLCM_ contrast, although in 3D analysis/manual of studies of patients with glioblastomas, which in our work we evaluated with the 3D semi-automated platform and observed significance related to progression-free survival of the radiomic characteristics GLCM_ContrastVariance and GLCM_correlation. A recent study published in January 2023 depicted the ability of GLCM radiomics to predict complete pathological responses in patients diagnosed with invasive breast cancer [43].

To emphasise the importance of the information obtained by radiomics, a need to implement the use of digital image terms such as voxels and discretised volumes, which are more precise than even cubic centimetres and more practical with values and cut-off points than support the best clinical practice for neurosurgery and radiotherapy management planning, was proposed. We observed a trend in this work suggested by other publications [44,45].

It has been described in the literature how radiomics models have the potential to assist clinicians in improving confidence in decision making in oncologic management [46].

Additionally, the publication of models depicting their verified negative and positive predictions of radiomics will have great potential to assist radio-oncologists, radiologists, and oncologists.

4.1. Limitations of the Study

Several limitations need to be addressed. We acknowledge the limited number of patients analysed. We found a lack of international consensus about the requirements and restrictions in extracting radiomic characteristics. The short evolution of the patients means that minimal information on the cases is described in clinical practice and, due to the neurological deterioration in the progression, fewer than expected studies can be obtained, including functional ones such as DTI, to evaluate more characteristics. In many cases, even performing an MRI is limited due to severe conditions, neurological deterioration, involuntary movements, and lack of time for the imaging assessment. Several patients identified were omitted because they had only undergone CT scans.

The scarcity of public databases prevents the analysis and comparison of data in search of the standardisation of strategies for the diagnostic and prognostic approach in these orphan pathologies, such as midline gliomas, in addition to the lack of a consensus for segmentation guides according to the published evidence of the ROI and radiomic profiles associated with prognosis and diagnosis.

Furthermore, in developing countries such as ours, accessibility to medical services affects early diagnoses and generates a concentration of patients with impaired initial functional status.

We did not use the radiotherapy targets gross tumour volume (GTV) or clinical target volume (CTV) contoured by the radio-oncologist manually, since these two variables were out of the scope of the research, as this could easily extend onto another manuscript.

It is important to remark that our study was performed with two MRI scanners. Our population could not perform the same analyses under more MRI scanners. Prior studies have evaluated the variability of results in radiomic studies according to the MRI and its selected scanner parameters [47–51]. The variations found are called the "scanner effect" and require harmonisation [52]. However, methods for bias correction to avoid this effect have also been studied with promising results [53–55]. We know this limitation needs to be better standardised for further application for radiomic models.

A severe difficulty we encountered during this research was the lack of descriptive studies that specifically focused on some of the mentioned radiomics (PARAMS_YSpatial Resampling, Conventional_peaksphere's). This is the reason why we were unable to compare our findings with other studies for all the radiomic features. To our knowledge, most studies report findings according to radiomic subgroups but not their performance.

4.2. Future Directions

For a better understanding and more complex research on orphan entities, it would be ideal to have an international data concentration centre where researchers from institutions worldwide could include their radiomic measurements from studies with a small number of patients. In this study, we were surprised that from only 12 patients and three tumour regions, over 5700 radiomic measurements were extracted. The amount of data that a multicentre study would generate with over 100 patients will also require dedicated computational power and a consensus for the radiomic measurements, extraction, analyses, use of machine learning, and other AI techniques.

Future studies should focus on the discretisation of the volumes and the base textures that, in this pathology, suggests quantified subunits of heterogeneities that will be relevant for the planning of oncological management [40]. There is a need for multicentre worldwide collaboration to find clues for progress and a race to improve these results for this group of patients. Proposals for algorithms and decision trees as guides for daily clinical practice with the evidence that is generated with more significant support by current publications in a cautious manner, mainly in an orphan entity such as the current one. To establish a better

consensus, further studies involving more extensive databases of patients are necessary, including patients with different variations of the H3F3A mutations.

5. Conclusions

There is a statistical trend for the role of first- and second-order radiomic features in influencing PFS and OS in this orphan entity. There is relevance for the GLCM texture profile, GLZLM_GLNU, and NGLDM_Contrast. The information found in this study could add to the existing evidence in the literature that would enrich the decision trees in the diagnosis and treatment of precision with the neuro-oncology team (neuroradiologists, neuropathologists, neurosurgeons, neuro-oncologists, paediatricians, and neurologists) and better support and perform precision medicine with fewer invasive procedures and the dose-paint technique for future radiotherapy treatment planning.

Author Contributions: Conceptualization, E.R.-V. and M.-F.C.-R.; methodology, E.R.-V. and M.-F.C.-R.; software, E.R.-V. and M.-F.C.-R.; validation, M.-F.C.-R. and S.M.-J.; formal analysis, M.G.-L. and E.R.-V.; investigation, M.-F.C.-R.; data curation, M.-F.C.-R. and S.M.-J.; writing—original draft preparation, M.-F.C.-R., M.G.-L. and E.R.-V.; writing—review and editing, M.-F.C.-R., M.G.-L. and E.R.-V.; visualization, M.G.-L.; supervision, M.-F.C.-R. and E.R.-V.; project administration, M.-F.C.-R. and E.R.-V. All authors have read and agreed to the published version of the manuscript.

Funding: This research received no external funding.

Institutional Review Board Statement: The study was conducted following the Declaration of Helsinki and approved by the Institutional Review Board of the National Committee of Scientific Research of Research of Oncology and paediatrics hospital of National Medical Centre S.XXI IMSS, Mexico City with F-CNIC-2020-321.

Data Availability Statement: The data used to support this study's findings are available from the corresponding author upon reasonable request.

Acknowledgments: Maria-Fatima Chilaca-Rosas was supported by Consejo Nacional de Ciencia y Tecnologia (CONACyT), Mexico, fellowship award CVU 426168. This work was submitted in partial fulfilment of the requirements for the DSc degree of Maria-Fatima Chilaca-Rosas at the Programa de Doctorado en Ciencias Medicas, Odontologicas y de la Salud, Universidad Nacional Autonoma de Mexico. M. G. L. was a research fellow at the directorate of research, Hospital General de Mexico, during 2022–2023.

Conflicts of Interest: The authors declare that there are no conflict of interest regarding the publication of this article.

References

1. Di Ruscio, V.; Del Baldo, G.; Fabozzi, F.; Vinci, M.; Cacchione, A.; de Billy, E.; Megaro, G.; Carai, A.; Mastronuzzi, A. Pediatric Diffuse Midline Gliomas: An Unfinished Puzzle. *Diagnostics* **2022**, *12*, 2064. [CrossRef] [PubMed]
2. Gianno, F.; Giovannoni, I.; Cafferata, B.; Diomedi-Camassei, F.; Minasi, S.; Barresi, S.; Buttarelli, F.R.; Alesi, V.; Cardoni, A.; Antonelli, M.; et al. Paediatric-type diffuse high-grade gliomas in the 5th CNS WHO Classification. *Pathologica* **2022**, *114*, 422–435. [CrossRef] [PubMed]
3. Mackay, A.; Burford, A.; Carvalho, D.; Izquierdo, E.; Fazal-Salom, J.; Taylor, K.R.; Bjerke, L.; Clarke, M.; Vinci, M.; Nandhabalan, M.; et al. Integrated Molecular Meta-Analysis of 1000 Pediatric High-Grade and Diffuse Intrinsic Pontine Glioma. *Cancer Cell* **2017**, *32*, 520–537.e5. [CrossRef]
4. Coleman, C.; Chen, K.; Lu, A.; Seashore, E.; Stoller, S.; Davis, T.; Braunstein, S.; Gupta, N.; Mueller, S. Interdisciplinary care of children with diffuse midline glioma. *Neoplasia* **2023**, *35*, 100851. [CrossRef]
5. Li, Q.; Dong, F.; Jiang, B.; Zhang, M. Exploring MRI Characteristics of Brain Diffuse Midline Gliomas With the H3 K27M Mutation Using Radiomics. *Front. Oncol.* **2021**, *11*, 646267. [CrossRef]
6. Singh, G.; Manjila, S.; Sakla, N.; True, A.; Wardeh, A.H.; Beig, N.; Vaysberg, A.; Matthews, J.; Prasanna, P.; Spektor, V. Radiomics and radiogenomics in gliomas: A contemporary update. *Br. J. Cancer* **2021**, *125*, 641–657. [CrossRef]
7. Preuss, K.; Thach, N.; Liang, X.; Baine, M.; Chen, J.; Zhang, C.; Du, H.; Yu, H.; Lin, C.; Hollingsworth, M.A.; et al. Using Quantitative Imaging for Personalized Medicine in Pancreatic Cancer: A Review of Radiomics and Deep Learning Applications. *Cancers* **2022**, *14*, 1654. [CrossRef]

8. Miranda, J.; Horvat, N.; Fonseca, G.M.; Araujo-Filho, J.D.A.B.; Fernandes, M.C.; Charbel, C.; Chakraborty, J.; Coelho, F.F.; Nomura, C.H.; Herman, P. Current status and future perspectives of radiomics in hepatocellular carcinoma. *World J. Gastroenterol.* **2023**, *29*, 43–60. [CrossRef]
9. Granata, V.; Caruso, D.; Grassi, R.; Cappabianca, S.; Reginelli, A.; Rizzati, R.; Masselli, G.; Golfieri, R.; Rengo, M.; Regge, D.; et al. Structured Reporting of Rectal Cancer Staging and Restaging: A Consensus Proposal. *Cancers* **2021**, *13*, 2135. [CrossRef]
10. Ma, Y.; Lin, Y.; Lu, J.; He, Y.; Shi, Q.; Liu, H.; Li, J.; Zhang, B.; Zhang, J.; Zhang, Y.; et al. A meta-analysis of based radiomics for predicting lymph node metastasis in patients with biliary tract cancers. *Front. Surg.* **2022**, *9*, 1045295. [CrossRef]
11. Gu, J.; Jiang, T. Ultrasound radiomics in personalised breast management: Current status and future prospects. *Front. Oncol.* **2022**, *12*, 963612. [CrossRef]
12. Coppola, F.; Faggioni, L.; Gabelloni, M.; De Vietro, F.; Mendola, V.; Cattabriga, A.; Cocozza, M.A.; Vara, G.; Piccinino, A.; Monaco, S.L.; et al. Human, All Too Human? An All-Around Appraisal of the "Artificial Intelligence Revolution" in Medical Imaging. *Front. Psychol.* **2021**, *12*, 710982. [CrossRef]
13. Kesler, S.R.; Harrison, R.A.; Rao, V.; Dyson, H.; Petersen, M.; Prinsloo, S. Predicting overall survival in diffuse glioma from the presurgical connectome. *Sci. Rep.* **2022**, *12*, 18783. [CrossRef]
14. Su, X.; Chen, N.; Sun, H.; Liu, Y.; Yang, X.; Wang, W.; Zhang, S.; Tan, Q.; Su, J.; Gong, Q.; et al. Automated machine learning based on radiomics features predicts H3 K27M mutation in midline gliomas of the brain. *Neuro Oncol.* **2020**, *22*, 393–401. [CrossRef]
15. Kandemirli, S.G.; Kocak, B.; Naganawa, S.; Ozturk, K.; Yip, S.S.; Chopra, S.; Rivetti, L.; Aldine, A.S.; Jones, K.; Cayci, Z.; et al. Machine Learning-Based Multiparametric Magnetic Resonance Imaging Radiomics for Prediction of H3K27M Mutation in Midline Gliomas. *World Neurosurg.* **2021**, *151*, e78–e85. [CrossRef]
16. Huang, W.-Y.; Wen, L.-H.; Wu, G.; Hu, M.-Z.; Zhang, C.-C.; Chen, F.; Zhao, J.-N. Comparison of Radiomics Analyses Based on Different Magnetic Resonance Imaging Sequences in Grading and Molecular Genomic Typing of Glioma. *J. Comput. Assist. Tomogr.* **2021**, *45*, 110–120. [CrossRef] [PubMed]
17. Zhou, W.; Huang, Q.; Wen, J.; Li, M.; Zhu, Y.; Liu, Y.; Dai, Y.; Guan, Y.; Zhou, Z.; Hua, T. Integrated CT Radiomics Features Could Enhance the Efficacy of (18)F-FET PET for Non-Invasive Isocitrate Dehydrogenase Genotype Prediction in Adult Untreated Gliomas: A Retrospective Cohort Study. *Front. Oncol.* **2021**, *11*, 772703. [CrossRef] [PubMed]
18. Tam, L.T.; Yeom, K.W.; Wright, J.N.; Jaju, A.; Radmanesh, A.; Han, M.; Toescu, S.; Maleki, M.; Chen, E.; Campion, A.; et al. MRI-based radiomics for prognosis of pediatric diffuse intrinsic pontine glioma: An international study. *Neurooncol. Adv.* **2021**, *3*, vdab042. [CrossRef] [PubMed]
19. Wu, C.; Zheng, H.; Li, J.; Zhang, Y.; Duan, S.; Li, Y.; Wang, D. MRI-based radiomics signature and clinical factor for predicting H3K27M mutation in pediatric high-grade gliomas located in the midline of the brain. *Eur. Radiol.* **2022**, *32*, 1813–1822. [CrossRef]
20. Guo, W.; She, D.; Xing, Z.; Lin, X.; Wang, F.; Song, Y.; Cao, D. Multiparametric MRI-Based Radiomics Model for Predicting H3 K27M Mutant Status in Diffuse Midline Glioma: A Comparative Study Across Different Sequences and Machine Learning Techniques. *Front. Oncol.* **2022**, *12*, 796583. [CrossRef]
21. Deng, D.-B.; Liao, Y.-T.; Zhou, J.-F.; Cheng, L.-N.; He, P.; Wu, S.-N.; Wang, W.-S.; Zhou, Q. Non-Invasive Prediction of Survival Time of Midline Glioma Patients Using Machine Learning on Multiparametric MRI Radiomics Features. *Front. Neurol.* **2022**, *13*, 866274. [CrossRef]
22. Wagner, M.W.; Namdar, K.; Napoleone, M.; Hainc, N.; Amirabadi, A.; Fonseca, A.; Laughlin, S.; Shroff, M.M.; Bouffet, E.; Hawkins, C.; et al. Radiomic Features Based on MRI Predict Progression-Free Survival in Pediatric Diffuse Midline Glioma/Diffuse Intrinsic Pontine Glioma. *Can. Assoc. Radiol. J.* **2023**, *74*, 119–126. [CrossRef] [PubMed]
23. Nioche, C.; Orlhac, F.; Boughdad, S.; Reuzé, S.; Goya-Outi, J.; Robert, C.; Pellot-Barakat, C.; Soussan, M.; Frouin, F.; Buvat, I. LIFEx: A Freeware for Radiomic Feature Calculation in Multimodality Imaging to Accelerate Advances in the Characterisation of Tumor Heterogeneity. *Cancer Res.* **2018**, *78*, 4786–4789. [CrossRef]
24. Nioche, C. LIFExAnalytics 2023. Available online: https://www.lifexsoft.org/ (accessed on 27 January 2023).
25. Durand-Munoz, C.; Flores-Alvarez, E.; Moreno-Jimenez, S.; Roldan-Valadez, E. Pre-operative apparent diffusion coefficient values and tumour region volumes as prognostic biomarkers in glioblastoma: Correlation and progression-free survival analyses. *Insights Imaging* **2019**, *10*, 36. [CrossRef]
26. Flores-Alvarez, E.; Durand-Muñoz, C.; Cortes-Hernandez, F.; Muñoz-Hernandez, O.; Moreno-Jimenez, S.; Roldan-Valadez, E. Clinical Significance of Fractional Anisotropy Measured in Peritumoral Edema as a Biomarker of Overall Survival in Glioblastoma: Evidence Using Correspondence Analysis. *Neurol. India* **2019**, *67*, 1074–1081.
27. Cortez-Conradis, D.; Favila, R.; Isaac-Olive, K.; Martinez-Lopez, M.; Rios, C.; Roldan-Valadez, E. Diagnostic performance of regional DTI-derived tensor metrics in glioblastoma multiforme: Simultaneous evaluation of p, q, L, Cl, Cp, Cs, RA, RD, AD, mean diffusivity and fractional anisotropy. *Eur. Radiol.* **2013**, *23*, 1112–1121. [CrossRef] [PubMed]
28. Archila-Rincon, L.M.; Del Carmen Garcia-Blanco, M.; Roldan-Valadez, E. Diagnostic performance of CT densities in selected gray- and white-matter regions for the clinical diagnosis of brain death: A retrospective study in a tertiary-level general hospital. *Eur. J. Radiol.* **2018**, *108*, 66–77. [CrossRef] [PubMed]
29. Park, S.H.; Goo, J.M.; Jo, C.-H. Receiver operating characteristic (ROC) curve: Practical review for radiologists. *Korean J. Radiol.* **2004**, *5*, 11–18. [CrossRef]

30. DeLong, E.R.; DeLong, D.M.; Clarke-Pearson, D.L. Comparing the areas under two or more correlated receiver operating characteristic curves: A nonparametric approach. *Biometrics* **1988**, *44*, 837–845. [CrossRef]
31. Metz, C.E. Basic principles of ROC analysis. *Semin. Nucl. Med.* **1978**, *8*, 283–298. [CrossRef]
32. Xie, T.; Chen, X.; Fang, J.; Kang, H.; Xue, W.; Tong, H.; Cao, P.; Wang, S.; Yang, Y.; Zhang, W. Textural features of dynamic contrast-enhanced MRI derived model-free and model-based parameter maps in glioma grading. *J. Magn. Reson. Imaging* **2018**, *47*, 1099–1111. [CrossRef] [PubMed]
33. Qi, X.X.; Shi, D.F.; Ren, S.X.; Zhang, S.Y.; Li, L.; Li, Q.C.; Guan, L.M. Histogram analysis of diffusion kurtosis imaging derived maps may distinguish between low and high grade gliomas before surgery. *Eur. Radiol.* **2018**, *28*, 1748–1755. [CrossRef] [PubMed]
34. Suh, H.B.; Choi, Y.S.; Bae, S.; Ahn, S.S.; Chang, J.H.; Kang, S.-G.; Kim, E.H.; Kim, S.H.; Lee, S.-K. Primary central nervous system lymphoma and atypical glioblastoma: Differentiation using radiomics approach. *Eur. Radiol.* **2018**, *28*, 3832–3839. [CrossRef]
35. Taylor, C.; Ekert, J.O.; Sefcikova, V.; Fersht, N.; Samandouras, G. Discriminators of pseudoprogression and true progression in high-grade gliomas: A systematic review and meta-analysis. *Sci. Rep.* **2022**, *12*, 13258. [CrossRef]
36. Molina, D.; Pérez-Beteta, J.; Luque, B.; Arregui, E.; Calvo, M.; Borrás, J.M.; López, C.; Martino, J.; Velasquez, C.; Asenjo, B.; et al. Tumour heterogeneity in glioblastoma assessed by MRI texture analysis: A potential marker of survival. *Br. J. Radiol.* **2016**, *89*, 20160242. [CrossRef]
37. Shur, J.D.; Doran, S.J.; Kumar, S.; ap Dafydd, D.; Downey, K.; O'Connor, J.P.B.; Papanikolaou, N.; Messiou, C.; Koh, D.-M.; Orton, M.R. Radiomics in Oncology: A Practical Guide. *Radiographics* **2021**, *41*, 1717–1732. [CrossRef]
38. Soni, N.; Priya, S.; Bathla, G. Texture Analysis in Cerebral Gliomas: A Review of the Literature. *AJNR Am. J. Neuroradiol.* **2019**, *40*, 928–934. [CrossRef]
39. Tomaszewski, M.R.; Gillies, R.J. The Biological Meaning of Radiomic Features. *Radiology* **2021**, *299*, E256. [CrossRef]
40. Lohmann, P.; Franceschi, E.; Vollmuth, P.; Dhermain, F.; Weller, M.; Preusser, M.; Smits, M.; Galldiks, N. Radiomics in neuro-oncological clinical trials. *Lancet Digit. Health* **2022**, *4*, e841–e849. [CrossRef]
41. Gillies, R.J.; Kinahan, P.E.; Hricak, H. Radiomics: Images Are More than Pictures, They Are Data. *Radiology* **2016**, *278*, 563–577. [CrossRef]
42. O'Byrne, M.; Ghosh, B.; Pakrashi, V.; Schoefs, F. Texture Analysis based Detection and Classification of Surface Features on Ageing Infrastructure Elements. In *BCRI2012 Bridge & Concrete Research in Ireland*; HAL Open Science: Lyon, France, 2012.
43. Syed, A.; Adam, R.; Ren, T.; Lu, J.; Maldjian, T.; Duong, T.Q. Machine learning with textural analysis of longitudinal multiparametric MRI and molecular subtypes accurately predicts pathologic complete response in patients with invasive breast cancer. *PLoS ONE* **2023**, *18*, e0280320. [CrossRef] [PubMed]
44. Kickingereder, P.; Isensee, F.; Tursunova, I.; Petersen, J.; Neuberger, U.; Bonekamp, D.; Brugnara, G.; Schell, M.; Kessler, T.; Folty, M.; et al. Automated quantitative tumour response assessment of MRI in neuro-oncology with artificial neural networks: A multicentre, retrospective study. *Lancet Oncol.* **2019**, *20*, 728–740. [CrossRef] [PubMed]
45. Shen, B.; Zhang, Z.; Shi, X.; Cao, C.; Zhang, Z.; Hu, Z.; Ji, N.; Tian, J. Real-time intraoperative glioma diagnosis using fluorescence imaging and deep convolutional neural networks. *Eur. J. Nucl. Med. Mol. Imaging* **2021**, *48*, 3482–3492. [CrossRef] [PubMed]
46. Ren, J.; Li, Y.; Yang, J.J.; Zhao, J.; Xiang, Y.; Xia, C.; Cao, Y.; Chen, B.; Guan, H.; Qi, Y.-F.; et al. MRI-based radiomics analysis improves pre-operative diagnostic performance for the depth of stromal invasion in patients with early stage cervical cancer. *Insights Imaging* **2022**, *13*, 17. [CrossRef] [PubMed]
47. Shiradkar, R.; Ghose, S.; Jambor, I.; Taimen, P.; Ettala, O.; Purysko, A.S.; Madabhushi, A. Radiomic features from pretreatment biparametric MRI predict prostate cancer biochemical recurrence: Preliminary findings. *J. Magn. Reson. Imaging* **2018**, *48*, 1626–1636. [CrossRef]
48. Moradmand, H.; Aghamiri, S.M.R.; Ghaderi, R. Impact of image preprocessing methods on reproducibility of radiomic features in multimodal magnetic resonance imaging in glioblastoma. *J. Appl. Clin. Med. Phys.* **2020**, *21*, 179–190. [CrossRef]
49. Um, H.; Tixier, F.; Bermudez, D.; Deasy, J.O.; Young, R.J.; Veeraraghavan, H. Impact of image preprocessing on the scanner dependence of multi-parametric MRI radiomic features and covariate shift in multi-institutional glioblastoma datasets. *Phys. Med. Biol.* **2019**, *64*, 165011. [CrossRef]
50. Waugh, S.A.; Lerski, R.A.; Bidaut, L.; Thompson, A.M. The influence of field strength and different clinical breast MRI protocols on the outcome of texture analysis using foam phantoms. *Med. Phys.* **2011**, *38*, 5058–5066. [CrossRef]
51. Buch, K.; Kuno, H.; Qureshi, M.M.; Li, B.; Sakai, O. Quantitative variations in texture analysis features dependent on MRI scanning parameters: A phantom model. *J. Appl. Clin. Med. Phys.* **2018**, *19*, 253–264. [CrossRef]
52. Saint Martin, M.J.; Orlhac, F.; Akl, P.; Khalid, F.; Nioche, C.; Buvat, I.; Malhaire, C.; Frouin, F. A radiomics pipeline dedicated to Breast MRI: Validation on a multi-scanner phantom study. *MAGMA* **2021**, *34*, 355–366. [CrossRef]
53. Shinohara, R.T.; Sweeney, E.M.; Goldsmith, J.; Shiee, N.; Mateen, F.J.; Calabresi, P.A.; Jarso, S.; Pham, D.L.; Reich, D.S.; Crainiceanu, C.M.; et al. Corrigendum to "Statistical normalisation techniques for magnetic resonance imaging" [NeuroImage: Clinical 6 (2014) 9-19]. *Neuroimage Clin.* **2015**, *7*, 848. [CrossRef] [PubMed]

54. Lin, M.; Chan, S.; Chen, J.-H.; Chang, D.; Nie, K.; Chen, S.-T.; Lin, C.-J.; Shih, T.-C.; Nalcioglu, O.; Su, M.-Y. A new bias field correction method combining N3 and FCM for improved segmentation of breast density on MRI. *Med. Phys.* **2011**, *38*, 5–14. [CrossRef] [PubMed]
55. Fortin, J.P.; Sweeney, E.M.; Muschelli, J.; Crainiceanu, C.M.; Shinohara, R.T.; Alzheimer's Disease Neuroimaging Initiative. Removing inter-subject technical variability in magnetic resonance imaging studies. *Neuroimage* **2016**, *132*, 198–212. [CrossRef]

Disclaimer/Publisher's Note: The statements, opinions and data contained in all publications are solely those of the individual author(s) and contributor(s) and not of MDPI and/or the editor(s). MDPI and/or the editor(s) disclaim responsibility for any injury to people or property resulting from any ideas, methods, instructions or products referred to in the content.